Chapter 5

Synthesis and Characterization of Glass Fiber Reinforced BMI-Epoxy-Rochelle salt Composites

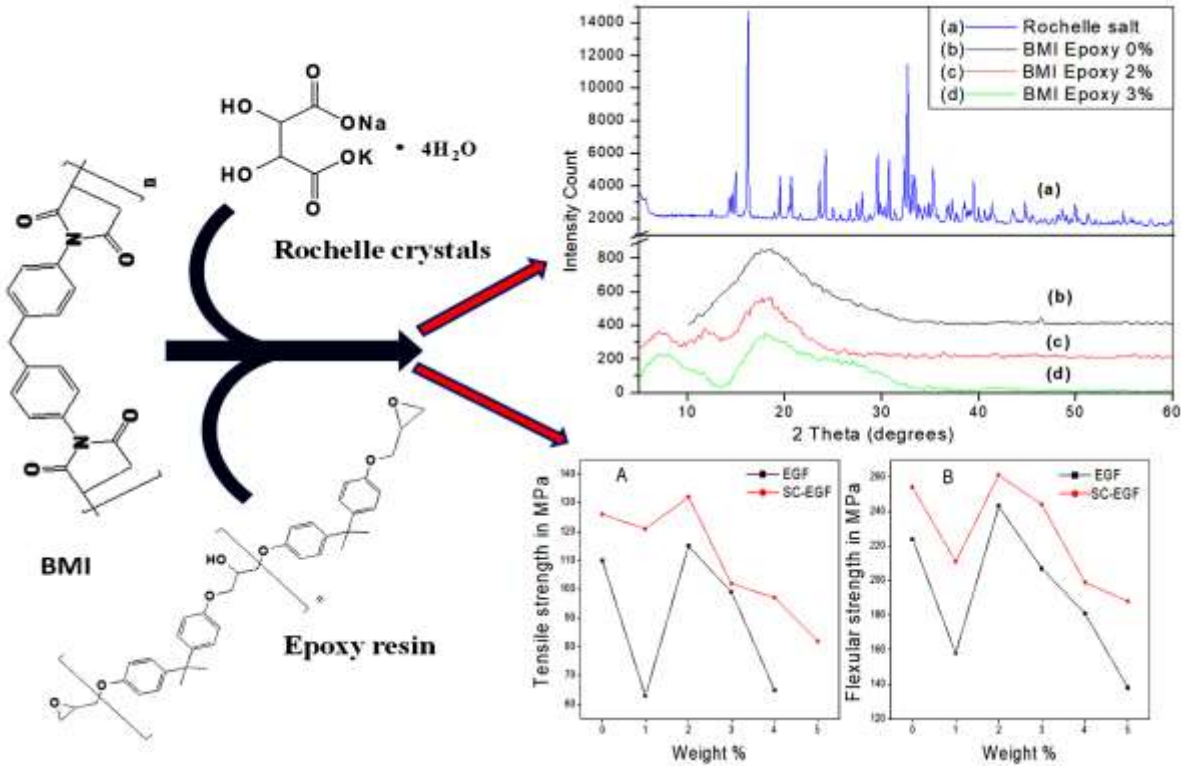

Chapter 5

Synthesis and Characterization of Glass Fiber Reinforced BMI-Epoxy-Rochelle Salt Composites

Abstract

In the present study, we developed a high performance Bismaleimide-epoxy-Rochelle salt filled (BMI-epoxy-RS) composites reinforced with E-glass fiber (EGF) and with silane coated E-glass fiber (SC-EGF) by employing simple hand layup method followed by compression moulding. With the addition of 2 weight % of RS filler, the composite demonstrated maximum increment in dielectric constant as well as in mechanical properties such as tensile and flexural strength. Composite with 3 weight % of RS filler exhibited high dielectric strength indicating this composition is more adaptable for high dielectric applications. Dielectric constants and dielectric loss of the fabricated composites have been obtained at higher frequencies (in GHz) using a vector network analyzer at room temperature and were found to be highest for the BMI-epoxy composite with 1% weight RS filler. Among the differently reinforced composites the one with SC-EGF as the reinforcement exhibit a significant increase in mechanical properties such as tensile strength and flexural strength which may be due to the interaction between matrix and silane functional groups on the glass fiber. The developed composite with low dielectric loss and high dielectric permittivity at room temperature can be applied in high dielectric applications.

5.1. Introduction

Being one of the most important high performance thermosetting resins, bismaleimide resin (BMI) has several applications in electronics, radar[1], capacitors[2], stealth technologies[3], circuit boards[4], microelectronics etc[5,6]. Different approaches like blending with rubber, thermoplastics, thermosets and reinforcement with glass fiber, carbon fiber etc. may be adopted to overcome the brittle nature of the cured resin. Epoxy resins are the widely used thermosetting matrix materials for high performance advanced composites. Epoxies are widely accepted in the aerospace industry for manufacturing composite parts because of their excellent mechanical properties, ease of manufacture, and suitable service temperature. BMI composites possess higher mechanical properties than

epoxy and are more efficient than the corresponding epoxy in high temperature applications. In order to achieve both the temperature performance of the BMI resin and the processing ease of epoxy resins, attempts have been made to prepare BMI-epoxy composites[7,8]. The thermal, mechanical and dielectric properties of the polymer composites strongly depend on the polymer matrix, size and weight percentage of the filler materials. All these parameters are crucial for the fabrication of polymer composites and all these parameters should be optimized to develop a novel polymer nanocomposite.

The first piezoelectric material discovered was sodium potassium tartarate tetrahydrate, commonly known as Rochelle salt (RS) or Seignette salt used in gramophone pickups and microphones. Rochelle salt is highly soluble in water and deliquescent. So in damp conditions, transducers made of this material may deteriorate. Being the only known, long time old ferroelectric, it finds several applications as laxative, in organic synthesis, in silvering of mirrors, ingredient of Fehling's solution, ingredient of Biuret reagent etc. [9,10]

Rochelle salt was the compound in which J. Valasek first recognized ferroelectric behaviour in 1920[11]. RS exhibited an unusual dielectric constant in the ferroelectric temperature from -40^{o}C to +40^{o}C. Andriy Andrusyk studied the piezoelectric effect of Rochelle salt based on Mitsui-type model and described the dielectric relaxation and thermodynamic properties along with ferroelectric phase transition at the microscopic level in Rochelle salt[12].

High dielectric permittivity materials have widespread applications in various fields like energy storage capacitors, micro capacitors in IC, sensors, printed circuit boards etc. The incorporation of high dielectric permittivity materials on the nanoscale into the polymer matrix could increase the dielectric constant of the polymer nanocomposites[13]. For high dielectric applications, the polymer composite should exhibit high dielectric permittivity, low dielectric loss and high dielectric breakdown strength[14–16]. High dielectric permittivity is highly desired for the dielectric materials used in the embedded capacitors and energy storage devices[17–19]. In order to enhance the dielectric properties of the BMI-epoxy composites, suitable fillers with high dielectric constants are added[20,21].

In the present work, the effect of RS filler loaded into BMI-epoxy composites reinforced with EGF and SC-EGF separately on the thermo-mechanical and dielectric properties is

investigated in detail. No similar studies regarding fabricated BMI-epoxy-RS composites have been reported before.

5.2. Results and discussion

5.2.1. FTIR analysis

5.2.1.1. Rochelle salt crystals

The FTIR spectrum of RS filler recorded in the range 400-4000 cm^{-1} is shown in figure 5.1 A. A very strong C=O stretching band at 1610 cm^{-1} confirms the presence of carboxylate anionic structure[22,23].

The strong peak at 1384 cm^{-1} is due to COO^- symmetric vibration. Strong C-H stretching peaks were observed at 1118 cm^{-1} and 2328 cm^{-1} whereas medium to weak peaks was at 2137, 1240 and 1211 cm^{-1}. The strong and sharp C-O stretching peak at 981 cm^{-1} indicates less interaction with the other groups in the crystal. The strong peak at 896 cm^{-1} corresponds to C-C stretching vibrations. The medium peaks at 613, 707 and 825 cm^{-1} correspond to the carboxylate anion. The low intensity O-H stretching vibration and strong O-H deformation appear at 3242, 3464 and 1051 cm^{-1} respectively (table 5.1).

Table.5.1 Important IR stretching frequencies of pure RS filler.

Wavenumber(cm^{-1})	intensity	Assignment
3464	weak	O-H Stretching
3242	Medium	O-H Stretching
2328	Strong	C-H Stretch
2137	Medium	C-H Stretch
1610	Very strong	C=O Stretch
1384	Strong	C=O / -COO
1240	Weak	C-H Stretch
1211	Weak	C-H Stretch
1118	Strong	C-H Stretch
1051	Strong	O-H deformation
981	Strong	C-O Stretching

896	Strong	C-C Stretch
825	Medium	δ_{coo}
707	Medium	τ_{coo}
613	Medium	τ_{coo}

5.2.1.2. BMI-epoxy composite and BMI resin

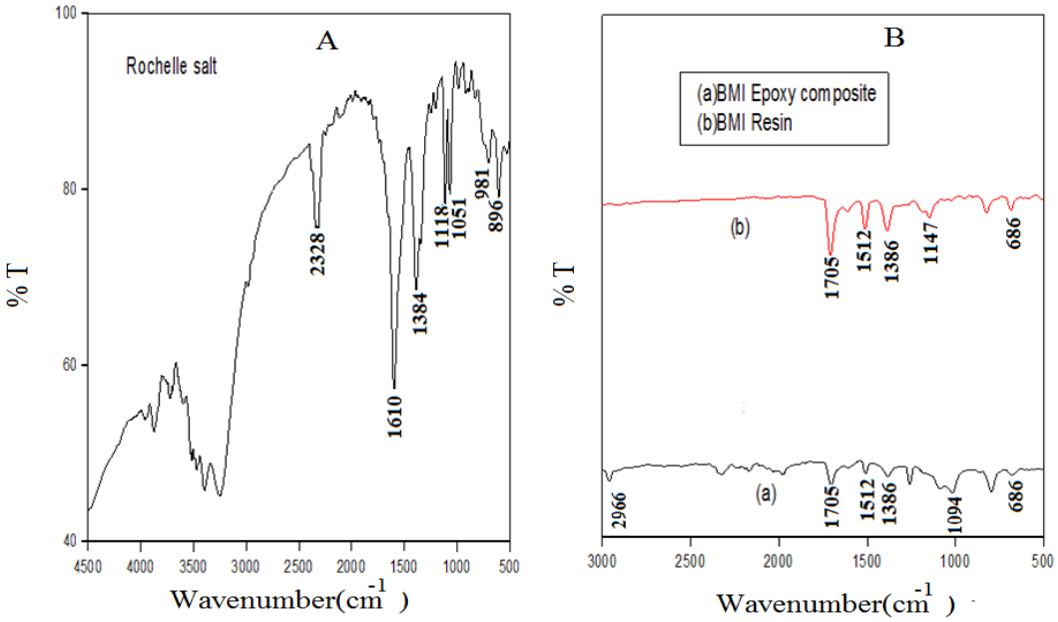

Figure 5.1 FTIR analysis of (A) RS filler (B) (a) BMI-epoxy composite (b) BMI resin.

FTIR spectra recorded for pure BMI resin and BMI-epoxy composite are shown in figure 5.1 B. A comparison of the peaks for pure BMI resin and BMI-epoxy composite reveals that the peaks correspond to (i) the maleimide benzene ring and imide group at 686 and 1386 cm^{-1} (ii) C=O group at 1705 cm^{-1} (iii) C=C benzene ring at 1512 cm^{-1} show no shift in bands. The following shift in bands was observed during the fabrication of BMI-epoxy composites: (i) strong peak corresponds to C-N-C maleimide group at 1147 cm^{-1} shifted to medium at 1094 cm^{-1} (ii) peak corresponds to -C-H maleimide group at 3101 cm^{-1} shifted to 2966 cm^{-1}.

5.2.1.3. BMI-epoxy-RS composites

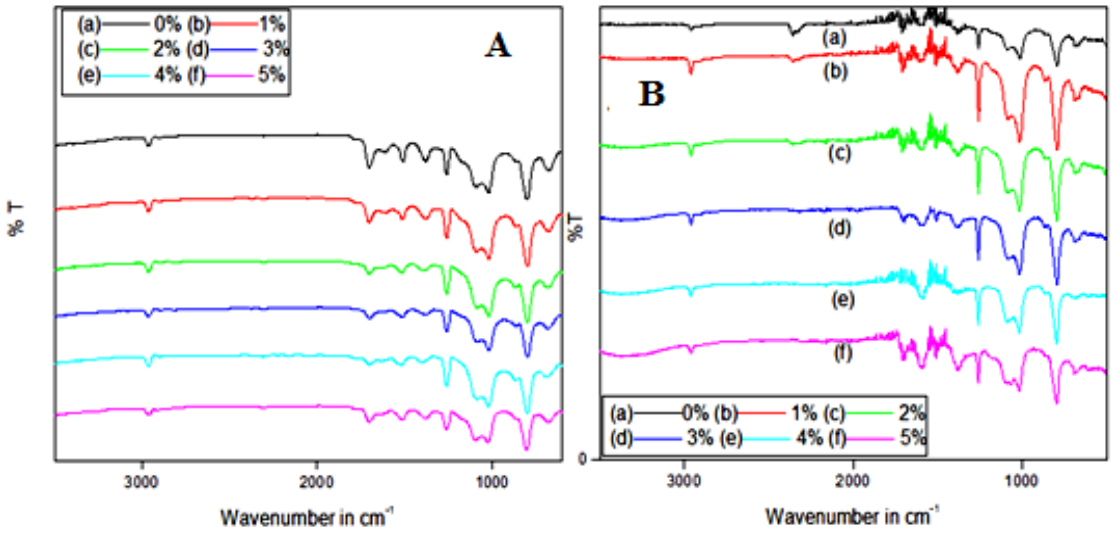

Figure 5.2 FTIR analysis of the BMI-epoxy-RS composites reinforced with (A) EGF (B) SC-EGF.

FTIR spectra of EGF and SC-EGF reinforced BMI-epoxy composites with varying weight percentages (1-5weight %) are shown in figure 5.2. Comparative studies reveal that the characteristic peaks are not significantly altered in differently reinforced BMI-epoxy RS composites. The IR peak for the oxirane ring of the epoxy resin is absent at 915 cm^{-1} in both BMI-epoxy composites with and without nanofiller (figure 5.1 B (a) & figure 5.2). This suggests the possibility of ring opening and consequent crosslinking between epoxy and BMI. Absorption in the region 2850-3000 cm^{-1} corresponds to C-H stretching. Wave numbers corresponding to epoxide ring vibrations (970, 862 and 1248 cm^{-1}) were also absent in the FTIR spectra of both BMI-epoxy composites with and without nanofiller further confirming the absence of epoxide ring. This indicates that during the fabrication of BMI-epoxy composites, inter crosslinking occurred between BMI and epoxy resin which proceeded through the ring opening of the epoxy oxirane ring and the formation of -N-CH(OH)CH_2- bonds between the nitrogen of maleimide ring and –CH of epoxy resin (refer chapter 4, figure 4.14)[24].

5.2.2. X-ray diffraction analysis

The semicrystalline nature of BMI has changed to amorphous when modified with epoxy resin (refer chapter 4, section 4.3.3.2 and figure 4.8) primarily because of the intercalation

of epoxy chains. Figure 5.3 A represents the X-ray diffractogram of RS. The crystallite size of the RS as determined using Debye Scherrer's equation was ~61.02 nm. The XRD pattern gave several sharp peaks confirming the crystalline nature of RS. Crystal planes corresponding to the observed prominent peaks of RS were identified and marked in the figure 5.3 A. Figure 5.3 B shows the XRD pattern of BMI-epoxy composite and BMI-epoxy composite loaded with 2 weight % RS as filler. It is clear from the diffractogram that RS loading into BMI-epoxy matrix has considerably altered the diffraction patterns of latter. The single halo peak extending from 2θ values 10° to 30° has split up into three peaks. In addition, some of the peaks corresponding to the crystal planes (410), (440), (512) etc., of RS are also visible. All these show that the crystallinity of BMI-epoxy composite has increased slightly upon RS loading. These observations further point out that RS was successfully incorporated into BMI-epoxy composite and an appreciable interaction existed between the composite and RS filler.

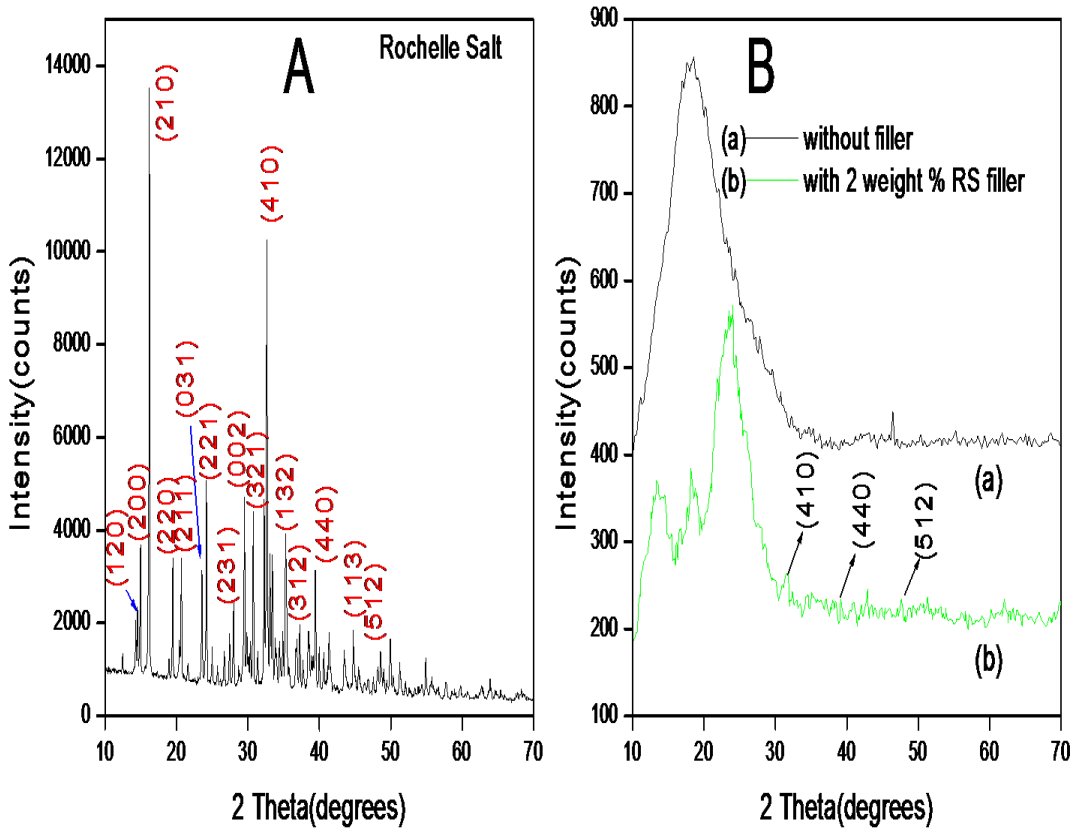

Figure 5.3 X-ray diffraction pattern of (A) Rochelle salt (B) BMI-epoxy composite (a) without RS (b) with 2 weight *% RS.*

Table 5.2 Comparison of 2θ and d values in BMI-epoxy-RS composites with 2 weight *% and 3* weight *% of RS filler*.

Rochelle salt		BMI-epoxy composites with			
		2 weight % RS filler		3 weight % RS filler	
2 θ	d (A°)	2 θ	d (A°)	2 θ	d (A°)
7.499	1.178	7.511	1.176	7.506	1.176
8.0209	1.104	8.004	1.1036	8.047	1.0977
18.0615	0.4908	18.07	0.4906	18.087	0.4901
18.4527	0.4805	18.471	0.4800	18.453	0.4793

5.2.3. Thermogravimetric analysis

The TGA curves of BMI resin, RS filler, BMI-epoxy composite and BMI-epoxy composite with 2 weight % RS filler are shown in figure 5.4. The TGA analysis was done between 30^0C to 750^0C at a heating rate of 20^0C per minute in nitrogen atmosphere. By comparative analysis of figure 5.4 A b, c and d, it is clear that the value of Tg goes on decreasing. BMI-epoxy composite with 2 weight % RS filler has a larger value of Tg due to the following reasons (1) Greater extent of cross links during curing (2) Incorporation of RS filler strengthens the intermolecular forces.

From the TGA curves in figure 5.4 A and table 5.3, it is clear that BMI-epoxy composite with 2 weight % RS has higher thermal stability compared to BMI resin and BMI-epoxy matrix. This can be attributed to the interaction of the dispersed RS nanofiller with adjacent polymer matrix layers.

Table 5.3 Weight loss percentages of samples obtained from TGA curves.

Sample	Total weight % at 661°C	T 5% (Initial thermal decomposition temperature)
BMI resin	39	362°C
BMI-epoxy composite without filler	45	368°C
BMI-epoxy composite with 2 weight % of RS filler	47	374°C

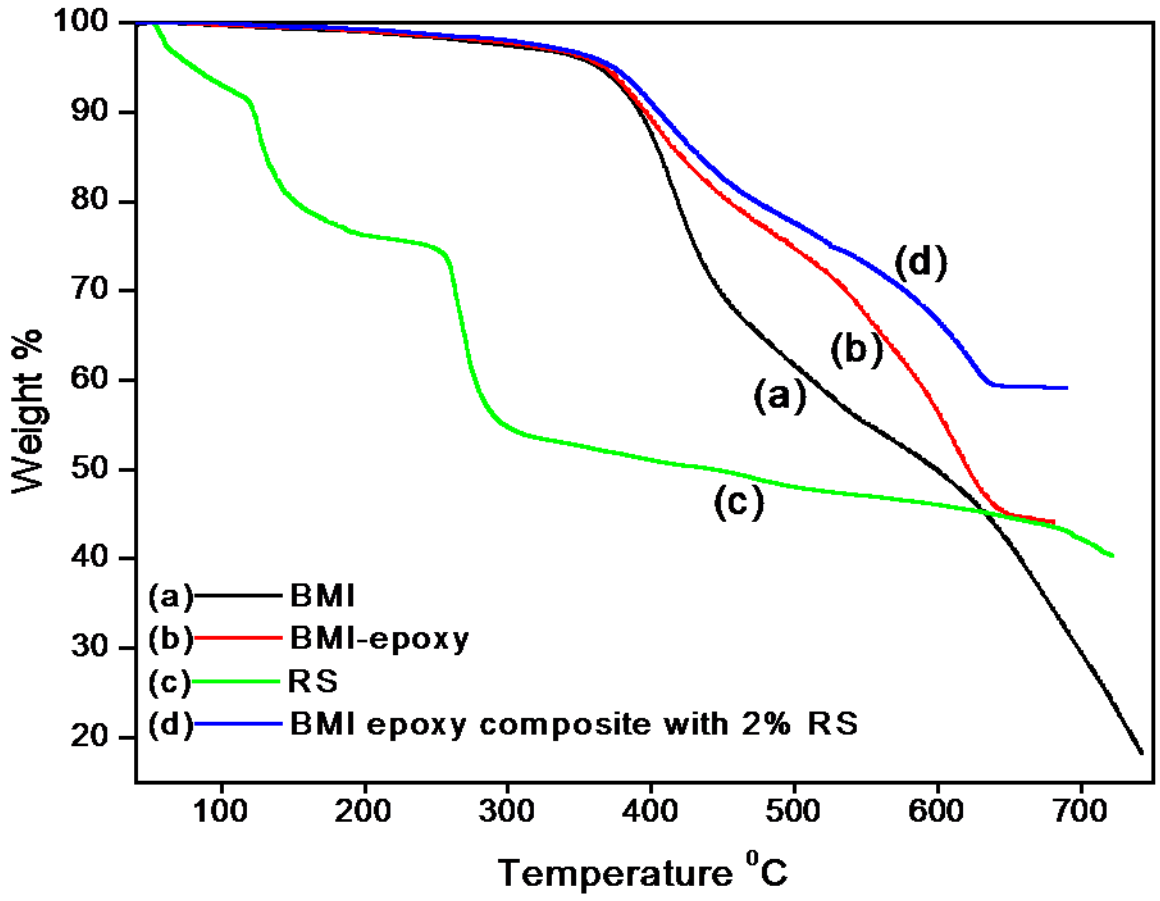

Figure 5.4 TGA curves of (a) BMI resin (b) BMI-epoxy composite without RS filler (c) RS filler (d) BMI-epoxy composite with 2 weight % RS filler.

5.2.4. Morphology of Rochelle salt crystals and BMI-epoxy-RS composites

SEM image of RS filler (figure 5.5 A) revealed that the lattice is composed of polydispersed particles with diameters varying from 1µm-10µm with a sphere like morphology. The morphological variation of BMI resin (figure 5.5 C) as well as BMI-epoxy composite (figure 5.5 D) was discussed in detail in chapter 4, section 4.3.2, figure 4.5. Figure 5.5 E and F represent the cross-sectional SEM images of BMI-epoxy composites loaded with 2 and 3 weight % of RS filler. BMI-epoxy composite with 2 weight % of RS filler possesses a uniform smooth surface that reveals the homogeneous dispersion of RS filler. EDAX pattern of RS filler (figure 5.5 B) showed the presence of carbon, oxygen, sodium, potassium and silicon with atomic percentages of 56.40, 36.69, 2.77, 3.31 and 0.83 respectively.

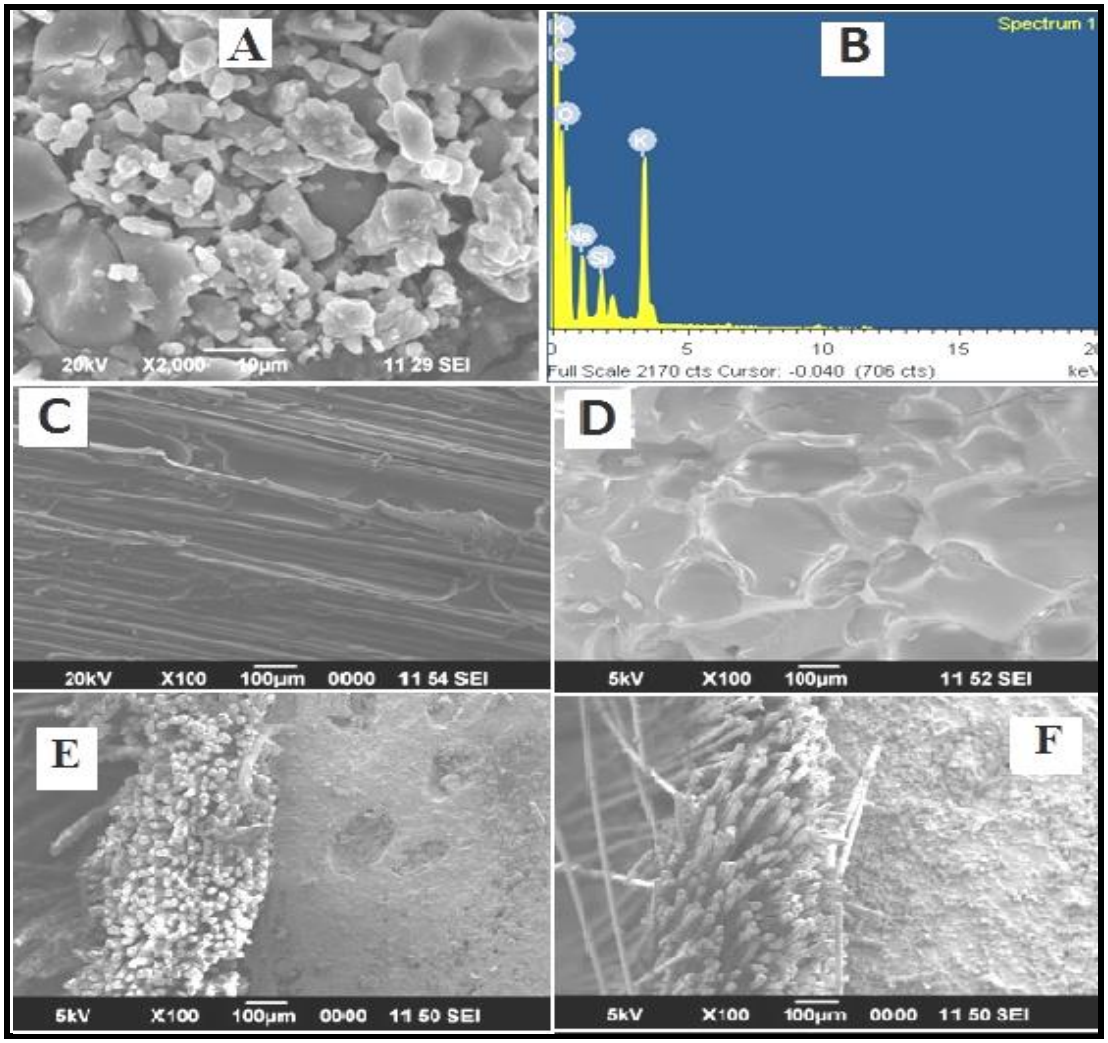

Figure 5.5 SEM images of (A) RS filler, (C) BMI-epoxy composite without filler, (D) BMI resin, Cross sectional SEM images of BMI-epoxy nanocomposites with (E) 2 weight *% (F) 3* weight *% of RS filler and (B) EDAX of RS filler.*

EDAX spectra of the fabricated BMI-epoxy composite with 3 weight % of RS filler (figure 5.6 a) confirmed the presence of carbon, oxygen, sodium and potassium in the sample. However, traces of silicon could also be observed in the spectra. EDAX mapping image of BMI-epoxy-RS composite (figure 5.6 b) shows the dispersion of various elements throughout the composite matrix. Figures 5.6 c, 5.6 d and 5.6 e further show the dispersion of individual elements, i.e., carbon, nitrogen and oxygen respectively in the composite. The mapping image of these elements does not show any aggregation, indicating uniform dispersion of RS filler along BMI-epoxy composite matrix.

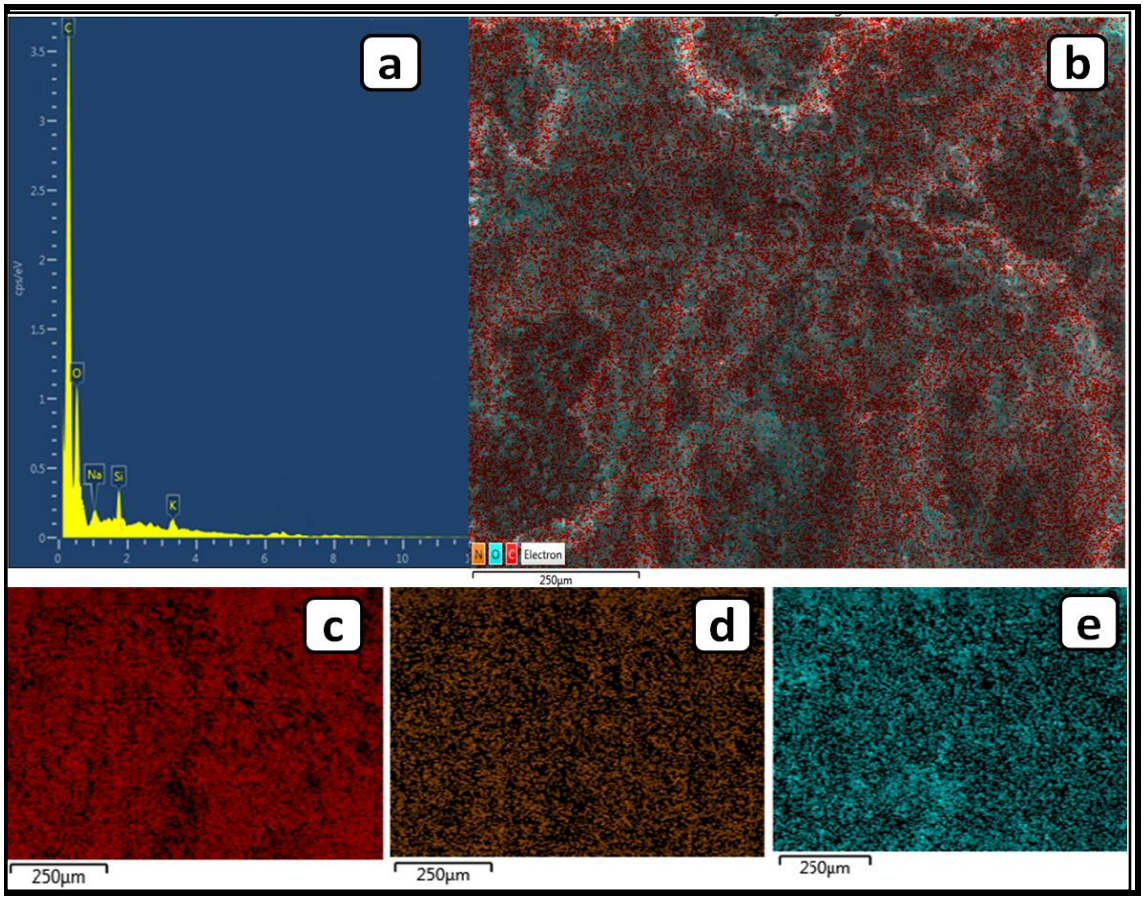

Figure 5.6 (a) EDAX spectra and EDAX mapping of BMI-epoxy composite with 3 weight % RS filler (b) EDAX mapping of carbon (c), nitrogen (d) and oxygen (e).

5.2.5. Mechanical properties of BMI-epoxy-RS composites

Figure 5.7 represents flexural and tensile strength measurements of BMI-epoxy-RS composites as per ASTM standards. The flexural and tensile strength of BMI-epoxy-RS composites was higher than that of BMI-epoxy composite without filler. The maximum value of tensile strength and flexural strength was obtained when the weight % of RS filler was 2 weight %. This may be due to the uniform distribution of nanofiller in the BMI-epoxy matrix with less agglomeration that facilitates better interaction between the polymer matrix and nanofiller.

The comparative analysis of the above test results showed a remarkable increase in the tensile and flexural strength of silane coated E-glass fiber reinforced nanocomposite, establishing that there is greater interaction between silane coated E-glass fiber and the polymer matrix[25].

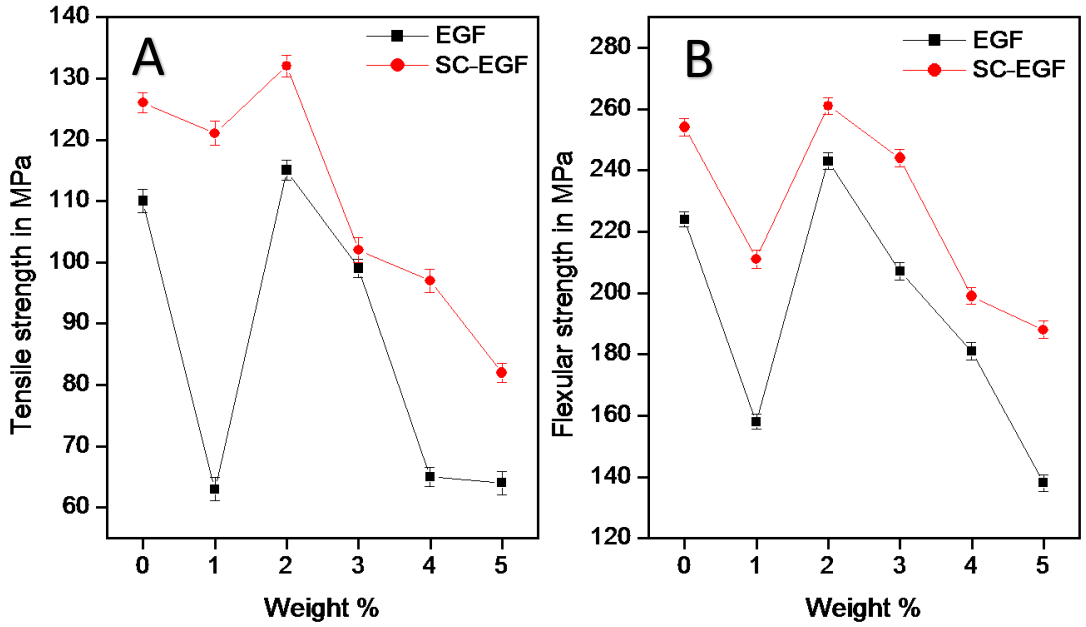

Figure 5.7 Comparative study of the effect of weight % of RS filler on A) tensile strength and B) flexural strength of BMI-epoxy-RS composites reinforced with EGF and SC-EGF.

5.2.6. Dielectric properties of BMI-epoxy-RS composites

5.2.6.1. Dielectric permittivity

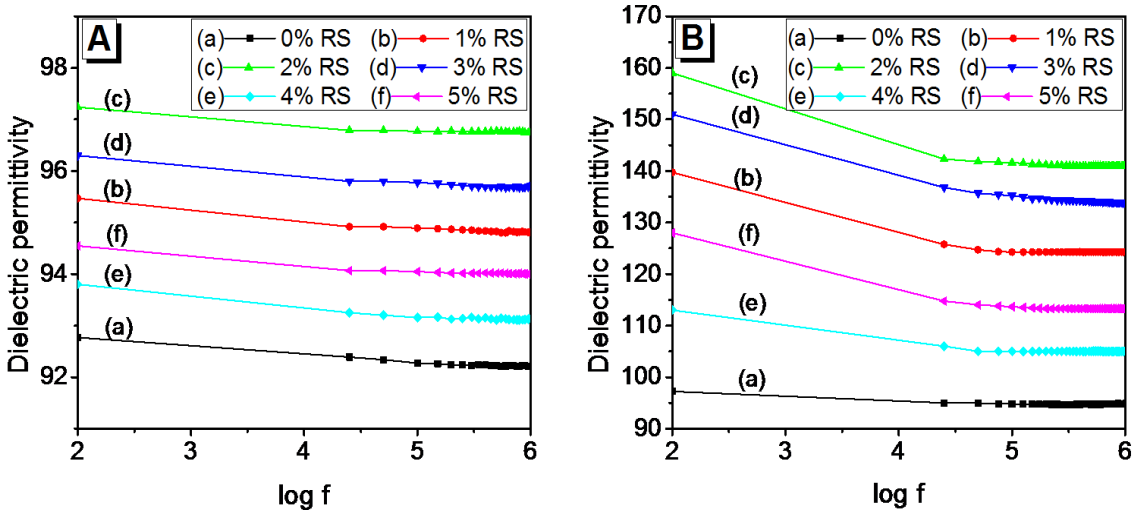

Figure 5.8 Variation of dielectric permittivity with logarithmic frequency of BMI-epoxy-RS composites reinforced with (A) EGF (B) SC-EGF.

The studies were carried out at room temperature for the frequency range from 102 to 106 Hz. The plots of dielectric permittivity for the BMI-epoxy-RS composites with varying weight percentage of RS filler are shown in figure 5.8. Experimental values of dielectric

constant showed a decreasing trend with an increase in frequency as we expect in most of the dielectric materials which may be due to interfacial relaxation (refer chapter 4, section 4.3.6.1). The maximum value of dielectric constant is obtained for BMI-epoxy composite with 2 weight % of RS filler[26,27].

5.2.6.2. Dielectric loss (tan delta)

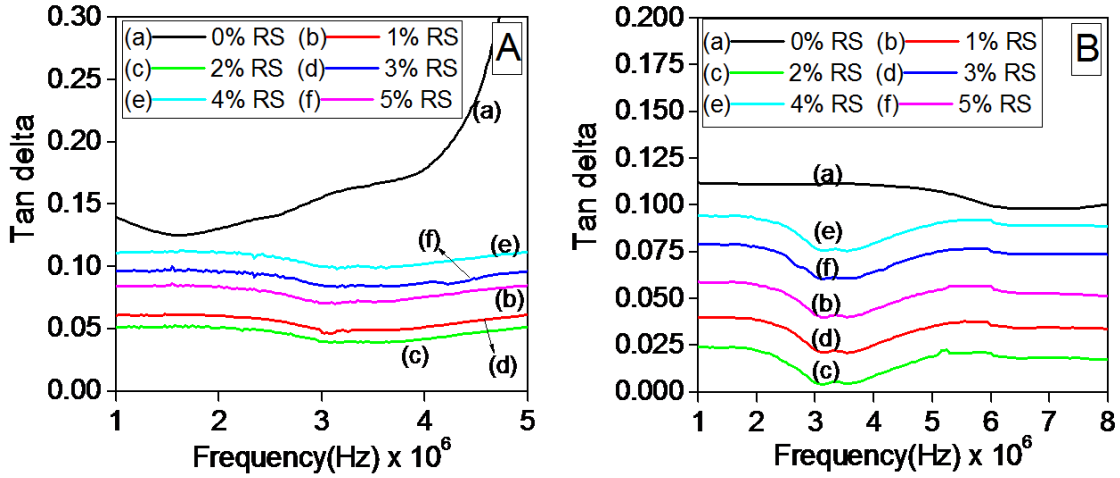

Figure 5.9 Frequency - tan delta graph of BMI-epoxy-RS composites reinforced with (A) EGF (B) SC-EGF.

Figure 5.9 shows the variation of dielectric loss with applied frequency for BMI-epoxy composites with 1-5 weight % of RS filler. At first, the dielectric loss of the fabricated composites decreases with an increase in frequency as expected due to the reduction of space charge polarization effect, reaches a minimum value and thereafter it increases with an increase in frequency. At higher frequencies, due to the charge accumulation at polar grain boundaries, polarization increases resulting in increased mobility of charge carriers leading to high dielectric loss[29]. At a very small ratio of RS (2 weight %), the dielectric loss of the composite remained very low.

5.2.6.3. Dielectric properties of BMI-epoxy-RS composites at high frequencies

Dielectric permittivity and dielectric loss of the nanocomposites have been determined at GHz frequencies (figure 5.10) using a vector network analyzer at room temperature[30]. Dielectric permittivity was highest and dielectric loss was lowest for the BMI-epoxy-RS composite with 1 weight % RS filler (refer chapter 4, section 4.3.6.3). High frequency will

disturb the already aligned dipoles in ferroelectric material and the reorientation of dipoles will not be easier in an external field, leading to a decrease in dielectric permittivity.

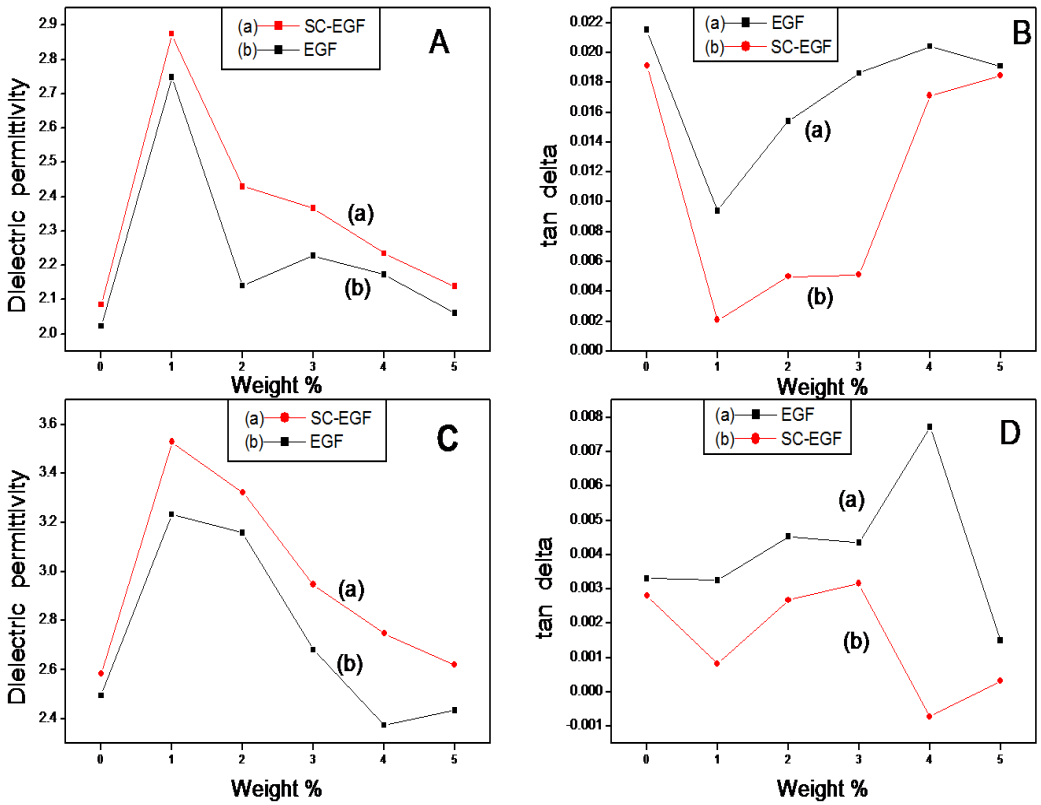

Figure 5.10 Dielectric permittivity and tan delta of BMI-epoxy-RS composites with EGF and SC-EGF at frequencies 3.42 GHz (A&B) and 5.68 GHz (C&D).

5.2.6.4. Dielectric strength

Dielectric strength of an insulating material depends on several factors like chemical structure, additives with different dielectric constant, structural irregularities, interfacial interactions between the polymer matrix and filler/additive, distortion of electric field due to the difference in dielectric permittivities of the polymer matrix and the filler, degree of crystallinity etc. Figure 5.11 represents the effect of the weight % of RS filler on dielectric strength of BMI-epoxy-RS composites. The energy storage capacity and energy density of polymer nanocomposites depend upon the value of dielectric break down strength. Glass fiber reinforced (EGF and SC-EGF) BMI-epoxy-RS composites with 3 weight % of RS filler have better insulating properties. The increase in dielectric strength may be due to the synergic effect of uniform dispersion of the filler in BMI-epoxy matrix as well as the reduction in the mobility of the polymer chains as a result of interaction of RS filler with

BMI-epoxy matrix through hydrogen bonding.

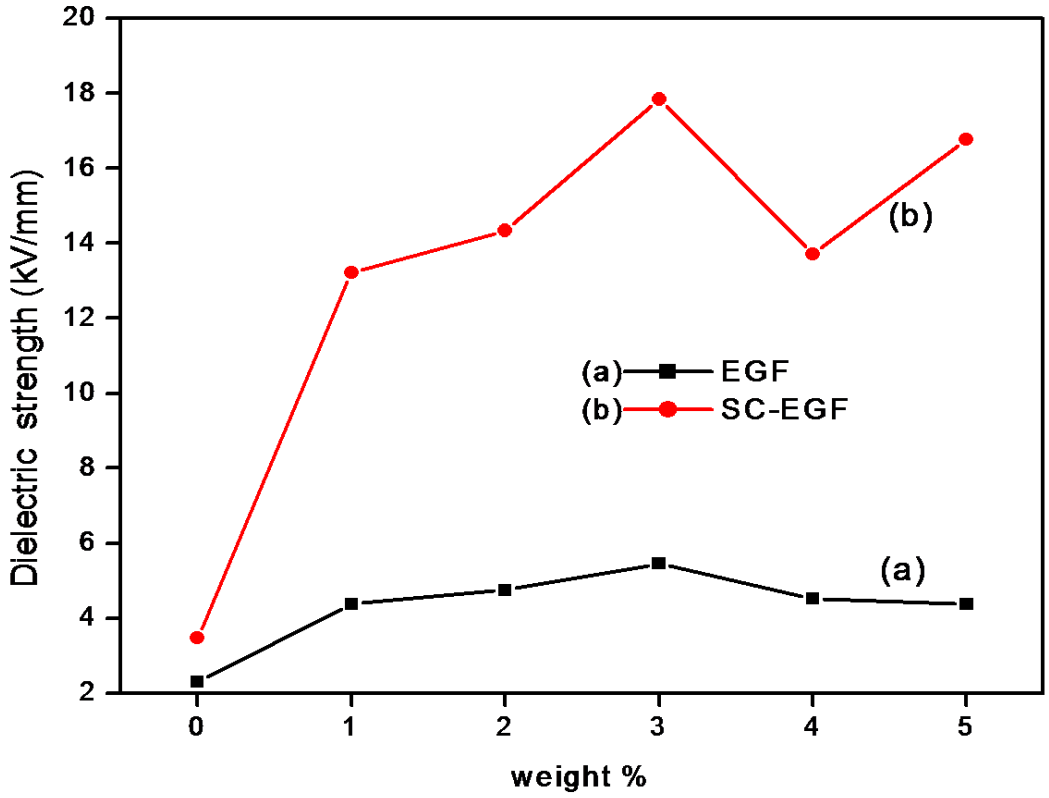

Figure 5.11 Effect of weight % of RS filler of BMI-epoxy composites reinforced with both EGF and SC-EGF on dielectric strength.

5.3. Conclusions

In this research work, both EGF and SC-EGF reinforced BMI-epoxy composites and BMI-epoxy composites with RS filler at different loadings were prepared and the effects of differently loaded RS filler on the mechanical, thermal and dielectric properties of BMI-epoxy composites were studied. Both EGF and SC-EGF reinforced BMI-epoxy-RS composites with 3 weight % of RS filler have better insulating properties and with 2 weight % of RS filler have better dielectric and mechanical properties. The mechanical and dielectric properties enhancement may arise from the synergic effect of uniform dispersion of RS filler and comparatively strong interaction between the polymer matrix and RS filler. Tensile strength of BMI-epoxy composite with 2 weight % RS nanofiller was increased 1.05 and 3.34 times both in EGF and SC-EGF reinforced composites whereas the flexural strength of the above composite was increased 1.085 and 4.24 times respectively with EGF and SC-EGF reinforcement as compared to BMI-epoxy composite

without filler. The enhancement in dielectric strength of BMI-epoxy composite with 2 weight % RS filler was found to be 2.37 and 4.17 times respectively with EGF and SC-EGF reinforcement compared to BMI-epoxy composite without filler. This significant enhancement in tensile and flexural strength as well as in breakdown voltage may be due to greater interaction between SC-EGF and BMI-epoxy matrix. Among the differently reinforced composites, the one with SC-EGF reinforced showed remarkable enhancement in both mechanical and dielectric properties that may be due to greater interaction between SC-EGF and the BMI-epoxy matrix. The maximum value of dielectric constant and minimum value of dielectric loss is obtained for BMI-epoxy composite with 2 weight % of RS filler. So, these composites can be applied in high dielectric application devices.

References

1. Jayalakshmi, C. G., Inamdar, A., Anand, A. & Kandasubramanian, B. Polymer matrix composites as broadband radar absorbing structures for stealth aircraft. J. Appl. Polym. Sci. 136, 47241 (2019).
2. Kakimoto, M. et al. Polymer-ceramic nanocomposites based on new concepts for embedded capacitor. Mater. Sci. Eng. B 132, 74–78 (2006).
3. Mangalgiri, P. D. Polymer-matrix composites for high-temperature applications. Def. Sci. J. 55, 175 (2005).
4. Fernandes, E. G., Tramidi, C., Gregorio, G. M. Di & Angeloni, G. Effect of Temperature-Pressure Cycles on Structural Properties of Epoxy-Based Composites for Printed Circuit Boards Applications. Appl. Polym. Sci. 110, 1606–1612 (2008).
5. Hu, J., Gu, A., Liang, G., Zhuo, D. & Yuan, L. Preparation and properties of mesoporous silica/bismaleimide/diallyl bisphenol composites with improved thermal stability, mechanical and dielectric properties. Express Polym. Lett. 5, 555–568 (2011).
6. Iredale, R. J., Ward, C. & Hamerton, I. Modern advances in bismaleimide resin technology: A 21st century perspective on the chemistry of addition polyimides. Prog. Polym. Sci. 69, 1–21 (2017).
7. Chandra, R. & Rajabi, L. Recent Advances in Bismaleimides and Epoxy-Lmide/ Bismaleimide Formulations and Composites. J. Macromol. Sci. Part C Polym. Rev. 37, 61–96 (1997).
8. Rajabi, L. & Malekzadeh, G. Effects of bismaleimide resin on dielectric and dynamic mechanical properties of epoxy-based laminates. Iran. Polym. J. (English Ed. 15, 447–455 (2006).
9. Lemaire, E., Moser, R., Borsa, C. J., Shea, H. & Briand, D. Green paper-based piezoelectric material for sensors and actuators. Procedia Eng. 120, 360–363 (2015).
10. Lemaire, E., Ayela, C. & Atli, A. Eco-friendly materials for large area piezoelectronics: Self-oriented Rochelle salt in wood. Smart Mater. Struct. 27, (2018).
11. Valasek, J. The early history of ferroelectricity. Ferroelectrics 2, 239–244 (1971).
12. Andrusyk, A. Piezoelectric effect in Rochelle salt. Ferroelectrics-Physical Effects (InTech Croatia, 2011).
13. Phougat, N., Vasudevan, P. & Nalwa, H. S. Handbook of Low and High Dielectric Constant Materials and Their Applications. vol. 1 (1999).
14. Mai, T. T. et al. Enhancement of polarization property of silane-modified $BaTiO_3$ nanoparticles and its effect in increasing dielectric property of epoxy/$BaTiO_3$ nanocomposites. J. Sci. Adv. Mater. Devices 1, 90–97 (2016).
15. Gu, A. High performance bismaleimide/cyanate ester hybrid polymer networks with excellent dielectric properties. Compos. Sci. Technol. 66, 1749–1755 (2006).
16. Barber, P. et al. Polymer composite and nanocomposite dielectric materials for pulse power

energy storage. Materials vol. 2 (2009).
17. Zhu, X. et al. Fabrication of core-shell structured Ni@$BaTiO_3$ sca ff olds for polymer composites with ultrahigh dielectric constant and low loss. Compos. Part A 125, 105521 (2019).
18. Zhao, B. et al. A versatile foaming platform to fabricate polymer/carbon composites with high dielectric permittivity and ultra-low dielectric loss. J. Mater. Chem. A 7, 133–140 (2019).
19. Jia, Q., Huang, X., Wang, G., Diao, J. & Jiang, P. MoS2 nanosheet superstructures based polymer composites for high-dielectric and electrical energy storage applications. J. Phys. Chem. C 120, 10206–10214 (2016).
20. Hu, J., Gu, A., Liang, G., Zhuo, D. & Yuan, L. Preparation and properties of mesoporous silica/bismaleimide/diallyl bisphenol composites with improved thermal stability, mechanical and dielectric properties. Express Polym. Lett. 5, 555–568 (2011).
21. Lu, G. & Huang, Y. Preparation and characterization of Bismaleimide resin/titania nanocomposites via sol-gel process. arXiv Prepr. arXiv1304.7082 (2013).
22. Uddin, M. J., Middya, T. R. & Chaudhuri, B. K. Room temperature ferroelectric effect and enhanced dielectric permittivity in Rochelle salt/PVA percolative composite films. Curr. Appl. Phys. 13, 461–466 (2013).
23. Bhattacharjee, R., Jain, Y. S., Raghubanshi, G. & Bist, H. D. Laser Raman and infrared spectra of Rochelle salt crystals. J. Raman Spectrosc. 19, 51–58 (1988).
24. Maity, P., Kasisomayajula, S. V, Parameswaran, V., Basu, S. & Gupta, N. Improvement in surface degradation properties of polymer composites due to pre-processed nanometric alumina fillers. IEEE Trans. Dielectr. Electr. Insul. 15, 63–72 (2008).
25. Kanag, S. Y., Anandan, Y. K., Vaidyanath, P. & Baskar, P. Strength properties of coated E-glass fibres in concrete. Gradjevinar 68, 697–703 (2016).
26. Mansingh, A. & Bawa, S. S. Dielectric properties of compressed Rochelle-salt powders. Phys. Status Solidi 21, 725–731 (1974).
27. Sawyer, C. B. & Tower, C. H. Rochelle salt as a dielectric. Phys. Rev. 35, 269 (1930).